Title

A Study of Rock Avalanche Deposits in San Antonio Canyon, San Gabriel Mountains, California

Permalink

https://escholarship.org/uc/item/3cx7m4bv

Author

Gentile, Christopher Ryan

Publication Date

2018

Peer reviewed|Thesis/dissertation

UNIVERSITY OF CALIFORNIA
RIVERSIDE

A Study of Rock Avalanche Deposits in San Antonio Canyon, San Gabriel Mountains,
California

A Thesis submitted in partial satisfaction
of the requirements for the degree of

Master of Science

in

Geological Sciences

by

Christopher Ryan Gentile

December 2018

Thesis Committee:
      Dr. Nicolas Barth, Chairperson
      Dr. Peter Sadler
      Dr. Katherine Kendrick

The Thesis of Christopher Ryan Gentile is approved:

_____

_____

_____
Committee Chairperson

University of California, Riverside

ABSTRACT OF THE THESIS

A Study of Rock Avalanche Deposits in San Antonio Canyon, San Gabriel Mountains, California

by

Christopher Ryan Gentile

Master of Science, Graduate Program in Geological Sciences
University of California, Riverside, December 2018
Dr. Nicolas Barth, Chairperson

San Antonio Canyon is a region of steep slopes and high relief within the eastern San Gabriel Mountains of southern California. This study examines five rock avalanche deposits within the canyon which have been previously interpreted to have been deposited between 100 ka and 2.6 Ma. This study finds evidence that these deposits are up to three orders of magnitude younger than previously thought, and thus that the San Antonio Canyon is a more active, dynamic, and hazardous landscape than previously thought. This study compliments recent work in the central San Gabriel Mountains that suggests large landslides are an underappreciated Holocene landscape driver throughout the San Gabriel Mountains.

TABLE OF CONTENTS

LIST OF FIGURES

LIST OF TABLES

Introduction

California is known for its many natural hazards including earthquakes, coastal erosion, forest fires, and flash flooding. These hazards can induce other significant problems, such as landslides. Landslides in California have destroyed property and taken many lives. The ability to better understand the triggers and timing of landslide events, as well as the landscape effects and evolution of their deposits, is of utmost importance for public safety. Landslides are one of the more readily mitigated natural hazards. Gaining more clear insight into landslide behavior will help plan for safer infrastructure and protect lives. Although smaller landslides and debris flows occur more frequently than large landslides, understanding the frequency and trigger mechanisms for large landslides (and their secondary hazards like dammed lakes and sediment transport) is important.

The San Gabriel Mountains are located in Los Angeles County and western San Bernardino County; 85% of the San Gabriel Mountains drain into the Greater Los Angeles Metropolitan Area (population 18.7 million). San Antonio Canyon in the eastern portion of the San Gabriel Mountains has a high concentration of large rock avalanche deposits and so was chosen as a case study to understand the spatio-temporal relations of large landslide deposits.

Setting of San Antonio Canyon, San Gabriel Mountains

Tectonics

The San Gabriel Mountains are part of the Transverse Ranges that run west-east, at a high angle (Lifton & Chase, 1992) to the other Californian mountain ranges, which trend northwest-southeast. Paleomagnetic remanence indicates that the San Gabriel

Block, which includes the San Gabriel Mountains and Transverse Ranges, rotated and translated into its current configuration in two separate clockwise rotations at around 21 Ma and 11 Ma (Luyendyk, 1991; Nicholson et al., 1994). The San Gabriel Mountains started to be uplifted and exhumed about 12 Ma with an acceleration around 5-7 Ma (Mattie and Morton, 1993; Blythe et al., 2002).

The San Gabriel Mountains are situated between three major fault systems; the San Andreas fault system, San Jacinto fault system, and the Sierra Madre-Cucamonga fault system (Fig. 1). The San Andreas and San Jacinto fault systems produce mainly right-lateral strike-slip motion to the east translating the San Gabriel Mountains northward. The Sierra Madre-Cucamonga thrust fault system bounds the southern front of the range and drives the majority of the compression and uplift to the San Gabriel Mountains. The rate of compression across the eastern San Gabriel Mountains is approximately 3 mm/yr producing a similar component of uplift (Weldon and Humphreys, 1986). Uplift rates have been found to generally increase eastward along the Sierra Madre-Cucamonga fault system (Lifton & Chase, 1992). All three fault systems are within 16 km (10 miles) of the San Antonio Canyon and can produce earthquakes of M_w >7 for the Sierra Madre-Cucamonga fault (Tucker & Dolan, 2001), ~M_w 6.7 for the northern segment of the San Jacinto fault (Sykes & Nishenko, 1984), and M_w >7.5 for the San Andreas fault (Olsen et al., 2006). Each of these have a predicted probability of producing a magnitude 6.7 or greater earthquake in the next thirty years (Fig. 2).

Figure 1: Simplified geologic map of the eastern San Gabriel Mountains. San Antonio Canyon (marked by the yellow trace) follows the SACF (San Antonio Canyon Fault). The other major faults shown in this map are SMF (Sierra Madre Fault), CF (Cucamonga Fault), SAF (San Andreas Fault), SJF (San Jacinto Fault), and NSGF (North Branch San Gabriel Fault). Minor faults are as listed:

DF– Duarte Fault, GHF– Glen Helen Fault, ICF– Icehouse Canyon Fault, LF– Lytle Creek Fault, MFLCF– Middle Fork Lytle Creek Fault, PMF– Pine Mountain Fault, PF– Punchbowl Fault, RHF– Raymond Hill Fault, SCCF– Sawpit Canyon-Clamshell Fault, SDCF– San Dimas Canyon Fault, SJoF– San Jose Fault, SSGF– southern branch San Gabriel Fault, SF– Scotland Fault, SCF– Stoddard Canyon Fault, SRF– Sunset Ridge Fault, VCF– Vasquez Canyon

Figure 2: This is a Google Earth image showing the main faults that were modeled by the third Uniform California Earthquake Rupture Forecast (UCERF-3). The scale indicates the probability of an earthquake, magnitude 6.7 or higher, occurring within the next thirty years on these faults. The San Andreas Fault has higher than 10% chance while the Sierra Madre-Cucamonga and the San Jacinto Faults have approximately a 1% chance. San Antonio Canyon is marked by the dotted white line. Fault abbreviations correspond with Figure 1

Geology

The basement rocks of the San Gabriel Mountains are mostly fractured Paleozoic metamorphic and Mesozoic plutonic rocks with some presumed Precambrian metamorphic rocks as well (Morton et al., 1989). There are small amounts of Tertiary volcanic and sedimentary rocks present as well. The rocks in which landslides typically occur in are Cretaceous and Permo-Triassic granitic rocks, amphibolite-grade schist and quartzite, hornblende-biotite bearing gneiss, and mylonite outcrops according to Morton et al. (1989). Both metamorphic and plutonic rocks crop out within San Antonio Canyon.

Topography

Topographic relief increases eastward along the eastern San Gabriel Mountains (Fig. 4) with the highest peak being Mt. San Antonio (also known as Mt. Baldy) at 3049 m (Morton & Miller, 2006). John Muir (1918) noted how treacherously steep the San Gabriel Mountains hillslopes are calling them "exceptionally steep and insecure to the foot of the explorer." Many of the hillslopes are prone to debris flows and landslides because they are at or steeper than the angle of repose (Burns & Sauer, 1992; Morton & Miller, 2006). The headwaters of San Antonio Canyon are on the southern flanks of Mt. San Antonio. The canyon floor is typically 60 meters wide in the vicinity of Mt. Baldy Village and reaches up to 800 meters wide at the mouth of the canyon near Claremont. The slopes, which are comprised of felsic plutonic rocks and metamorphic rocks (Morton and Miller, 2006), have a mean angle of approximately 35° (Fig. 3), where the angle of repose for granite is about 40° (Ulrich, 1987). There are a significant number of slopes that are above the mean and beyond the angle of repose, with a maximum angle of 85°.

Apatite fission track analyses indicate the southeastern portion of the San Gabriel

Mountains is rapidly uplifting (Blythe et al., 2000; Morton et al., 1989). The steep slopes

in this area are underlain by fractured bedrock, one of the criteria for producing rock

avalanches (Keefer et al., 1984; Morton & Miller, 2006).
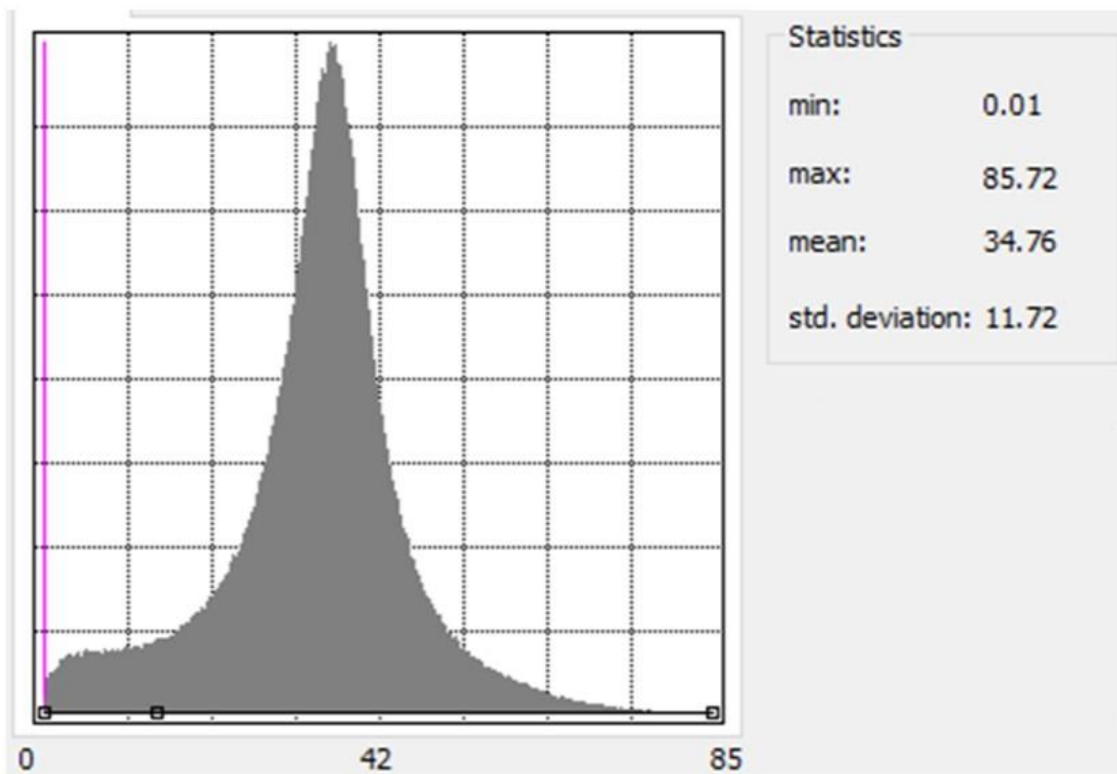
Figure 3. Histogram depicting the distribution of slope values for the San Antonio Canyon hillslopes.

Figure 4: The San Gabriel Mountains are an area of high elevation and steep slopes. This image shows slope overlain on a hillshade image from Cal-Topo (green: low slopes, red: steep slopes). The stars indicate the following locations: White— Crystal Lake rock avalanche deposit, Yellow— Mt. San Antonio Peak, Blue— Mt. Baldy Village, Black— San Antonio Dam.

Climate

The San Gabriel Mountains lie in a Mediterranean climate zone (Lifton & Chase, 1992) characterized by mild wet winters and hot dry summers. The San Gabriel Mountains cause uplift of winter westerly storm systems entering the Los Angeles Basin from the Pacific Ocean, leading to some of the highest hourly rainfall totals in the U.S. (Dr. Rich Minnich personal communication). Infiltration-excess resulting in overland flow may result, and is exacerbated if the soils have been saturated by prior storms (typically 10 inches of antecedent rainfall). The San Gabriel Mountains have a strong rain shadow effect on the northern side of the mountains. As humid air is uplifted over the southern side of the mountains, moisture is precipitated out of the air and warm, arid air sinks beyond the northern side of the mountains into the arid desert region of the Mojave Desert. The normal annual rainfall varies from 81 cm (32 in) at the mouth of the canyon to 110.5 cm (43.5 in) by Mt. Baldy Village (October 1996-September 2018) with an average creek discharge of 0.297 m^3/s (10.49 ft^3/s; 1918-1972) (NOAA, 2018; USGS, 2018).

During the Pleistocene, the climate was more humid in the San Gabriel Mountains, even at lower elevations which are arid today (Lifton & Chase, 1992). Precipitation was most likely high enough to support forests on both the south and north sides of the mountains until about 7.8 ka. However, from about 7.5 to 4.2 ka, there were warmer mean temperatures than at present that decreased plant cover and killed off trees at low altitude on south-facing slopes. Precipitation subsequently increased but trees are still scarce on south-facing slopes lower than 1300 m (Lifton & Chase, 1992). The early

Holocene has been suggested to be a wetter climate with higher rainfall rates than today and was drier than the Pleistocene according to lake deposit cores in North Fork San Gabriel Canyon (Crystal Lake) as well as dune activity and paleolakes from the Mojave Desert (Owen et al., 2003; Kirby et al., 2007; Tchakerian and Lancaster, 2002).

Vegetation

Chaparral, evergreen shrub species with thick leathery leaves (Stuart & Sawyer, 2001, p. 7), covers the majority of the San Gabriel Mountains (Fig. 5). There are thirteen native conifer tree species that are also present within the mountains (Burns & Sauer, 1992). Vegetation patterns are important indicators when searching for rock avalanche deposits due to variations in soil and drainage. The bouldery surfaces of young rock avalanche deposits lack well developed soils that can promote vegetation growth and the surfaces are relatively flat compared to the steep slopes of the canyon. Chaparral growth is limited on these surfaces. However, large conifers with deeper root systems such as Big-cone Douglas Fir grow readily in these low altitude settings, which is unusual when compared to the mountain range as a whole (Morton et al., 1989). The rubbly, well-drained slopes of the deposits also promote the growth of Canyon Live Oak. This contrasts with the surrounding areas where conifers are sparse, and chaparral is abundant at low-elevations of the mountains.
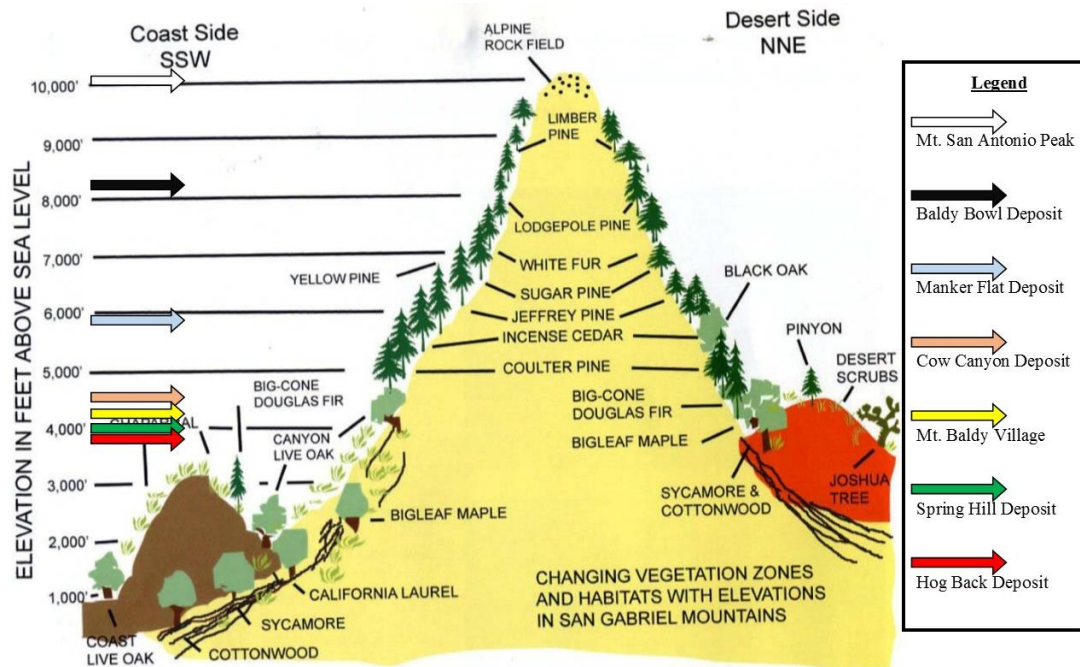
Figure 5: This image adapted from the Big Santa Anita Historical Society shows the changes in vegetation and habitat zone as elevation changes in the San Gabriel Mountains. The elevations of the five main rock avalanches have been added onto the figure, along with the elevation of Mt. Baldy Village and Mt. San Antonio Peak.

Landslide Categorization

Landslides are classified by material involved and the type of movement (Fig. 6) (Varnes, 1978). Landslide is a general term that describes several types of slope movement. The major modes of movement are flows, falls, topples, spreads, and slides. The three forms of material described are earth, debris, and rock. The landslides in this study are primarily composed of rock, but a brief introduction to debris flows is also given due to their local relevance.

Debris flows are typically triggered by heavy precipitation or a quick thaw of snow or frozen soil (Varnes, 1978). They are typically characterized by having large, unsorted rocks and boulders, along with wood material like tree trunks and branches, in a slurry of fine-grained clays and muds (Cannon & DeGraff, 2009). They are very rapid (5 cm/s) to extremely rapid (5 m/s) and move as a surging flow in steep channels (Hungr et

10

al., 2014). Debris flows are an important factor regarding both hazards and sediment supply in the San Gabriel Mountains (Lave & Burbank, 2004; Rulli and Rosso, 2005). Wildfires are prevalent in the San Gabriel Mountains during the long summer fire season and can contribute to increasing the amount of debris flows that occur in storm events in the following Winter (Lave & Burbank, 2004; Rulli and Rosso, 2005). Rulli and Rosso (2005) found that burning a catchment increases the rate of sediment production 7 to 35 times as much as an unburned catchment in the San Gabriel Mountains. Debris flows (called rapid soil flows by Keefer) can be triggered by earthquakes as well (Keefer, 1984).

Rock falls are loose, surficial rocks that are dislodged and fall directly below the source area (Varnes, 1978). Rock topples are a version of a rock fall where rock columns or walls separate from the main slope that rotate out from the slope but are still attached at the base. The base acts as a pivot point that the rock rotates over until the base breaks. Rock falls and topples are deposited close to the source area near the bottom of the slope (Varnes, 1978).

Rock slides are split into translational and rotational. Translational rock slides occur when the mass detaches and slides along a planar surface (Varnes, 1978). The deposition area can be near or far depending on the length of the slide surface. Rotational rock slides, also referred to as slumps, occur when the mass is back-rotated into its own collapsed area as it moves down a curved, concave-up, failure surface. This creates a depression at the head scarp where precipitation can accumulate and cause future movement. The toe of the rotational rock slide thrusts over the material that did not move

with the rock slide (Varnes, 1978). Rock falls can persist in unvegetated rock slide

headscarp areas.

All the above examples are end member slope failures.
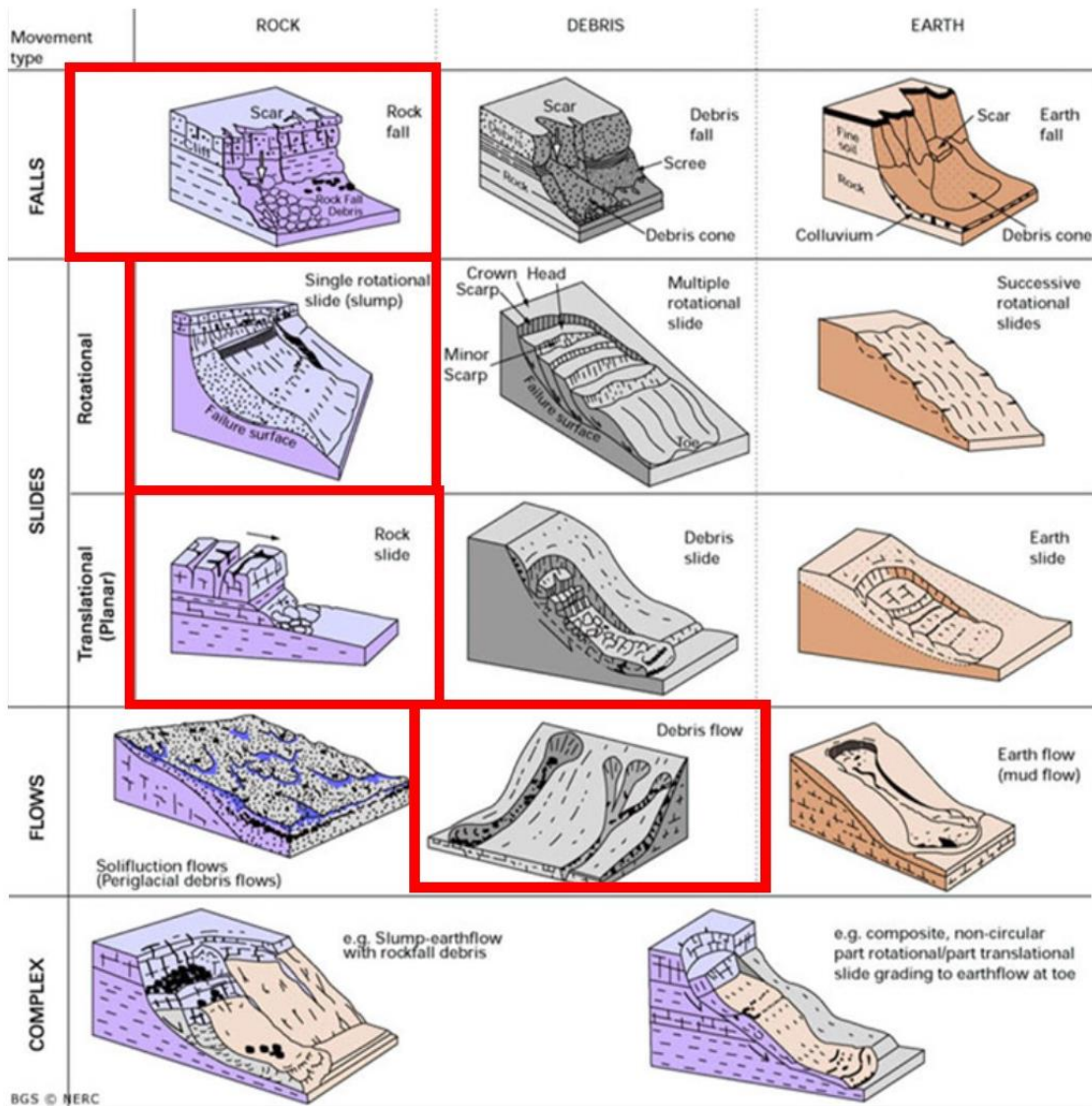
Figure 6: Landslide classification scheme produced by the British Geological Survey based on Varnes (1978) The landslide types that are important to this case study have been outlined in red. Rock avalanches can be considered complex, but they are more specifically a special type of rock slide. Complex landslides refer to events that have more than one type of movement involved.

Rock Avalanches

Any of the previously described movements can become more complex and turn into an avalanche. Rock avalanches, also known as sturzstroms, are complex landslides that represent an underappreciated hazard in California. They are the second deadliest mass movement triggered by earthquakes and require the strongest ground shaking for the longest duration to start moving (Keefer et al., 1984).

Rock avalanches are extremely rapid (>5 m/s), semi-coherently transported, fragmented rock that moves more like a fluid that can travel long distances (Hungr et al., 2001; Moore et al., 2017). They are typically triggered by large earthquakes that produce strong ground shaking in areas that have steep slopes and fractured bedrock (Keefer et al., 1984).

An idealized stratigraphy of rock avalanche deposits will have three basic layers (Fig. 7). Characteristically, there is almost no vertical mixing during transport such that original stratigraphy of the source area rock can be preserved; there is mainly shearing or fracturing, depending on the lithology, of the internal portions within the deposit (Fig. 8). There are three main layers described in the rock avalanche deposit stratigraphy: substrate (S), mixed zone (MZ), and boulder surface cap (BS). The term substrate is used in this context to describe the bottom-most layer that is mostly undisturbed with some shearing and jigsaw textures. The middle layer is the mixed zone is typically very thin, relative to the other layers, and is the only portion where there is some vertical mixing. This layer has shearing and jigsaw textures mixed with some material from the boulder

surface cap. The boulder surface cap (aka boulder cap) is the top layer and consists of loosely packed boulders with significant void space between them.
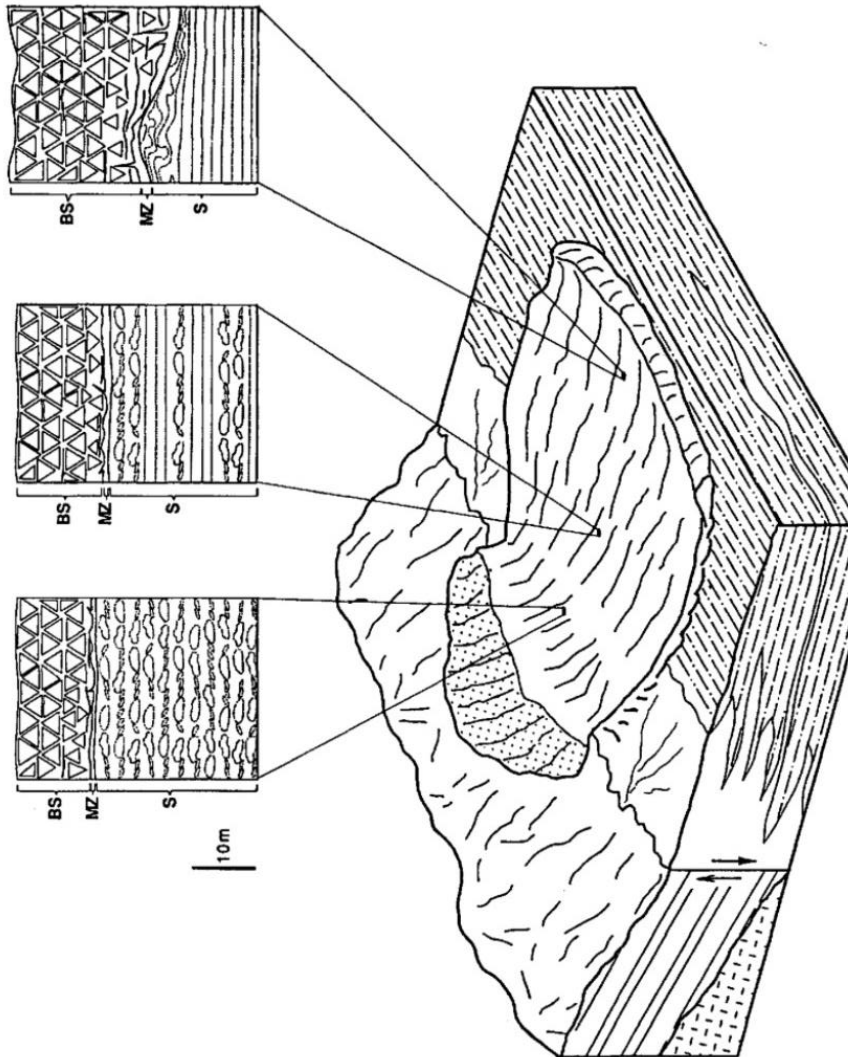
Figure 7: Schematic depicting a simple three layer stratigraphy of a rock avalanche deposit in a dry-climate (Yarnold & Lombard, 1989). The bottom most layer is the sheared zone, the middle layer is the mixed-zone, and the top layer is the boulder surface. This figure shows how the stratigraphy changes depending on whether the outcrop is distal, medial, or proximal. The proximal has mostly substrate with the boulder surface cap. The more distal the deposit, the more shearing and mixing occurs within the deposit. The boulder surface cap is thicker as well.
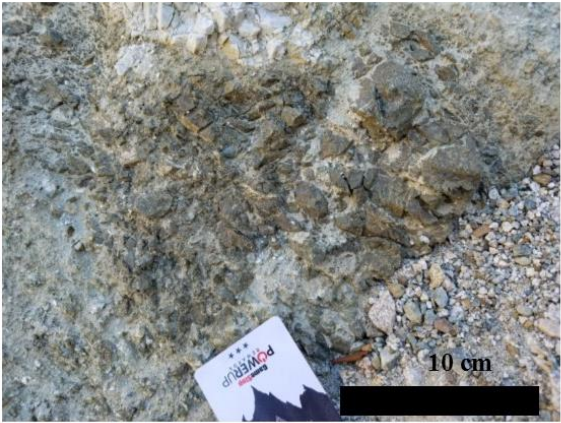
Figure 8: Rock avalanche textures. A) This is an example of shearing texture in the rock avalanche deposits. This comes from an older deposit closer to the mouth of the San Antonio Canyon that has lost its geomorphology and boulder cap. The outer portion of the white rock has been shattered and sheared off to the right. B) The rocks are shaken apart into this jigsaw puzzle texture wherein individual clasts are still able to be visually restored to create original rock as in a jigsaw puzzle. This texture is characteristic of the lower and mixed zone layers. This is an example from the Cow Canyon Saddle rock avalanche deposit. C) This is the surface of the Baldy Bowl rock avalanche deposit which shows the top portion of the boulder cap layer. The boulders are large and angular, showing little to no signs of weathering.

Rock Avalanche Hazards

Rock avalanche deposits within confined canyons can immediately disrupt the drainage system within the canyon. Deposits that travel down-valley tend to deflect the drainage, which can permanently disturb the river, or force the drainage to rework itself back to the original position. If the deposit does not move down valley, and instead moves laterally across the valley, the drainage can be dammed. This forms a lake upstream from the deposit, flooding valley bottom until the spillover elevation of the deposit is reached. The post-rock avalanche lake eventually breaches the deposit and normal down-canyon drainage resumes. The landslide deposit dam can benignly fail gradually or fail catastrophically unleashing a hazardous flood event. In either scenario the dam breach can cause large sediment pulses downstream of the deposit and create a knickpoint in the stream profile. In some cases of drainage deflection or damming, permanent drainage reorganization can occur. There is evidence presented by previous workers that the upstream catchment of the Mt. San Antonio and Icehouse Canyon catchments drained into the San Gabriel Canyon before the Cow Canyon Saddle rock avalanche (Morton et al., 1989; Morton & Miller, 2006).

Other hazards arising from rock avalanche deposits include an increase in mass wasting. The rock avalanche shakes and shears solid bedrock into a newly formed mass of unconsolidated fractured material. This material is now more easily weathered and eroded than surrounding bedrock with higher permeability. The availability of weaker rock increases sediment supply downstream, debris flow occurrences, smaller landslide occurrences, and erosion rates of knickpoints and knickzones.

Rock Avalanches and Landslides in the San Gabriel Mountains

The steep hillslopes, highly fragmented nature of the bedrock, and weak lithologies work together to produce a large number of landslides in the San Gabriel Mountains (Morton & Miller, 2006; Schmidt et al., 2011). Debris flows related to snow melt and post-wildfire rainfall occur annually in the San Gabriel Mountains and can threaten life and property. Creeping and slow-moving landslides are evidenced by bowed trees at the base and are underlain by the Cretaceous Pelona Schist (Morton & Miller, 2006). Sackungen features, both as side-hill and ridge-top trenches, are common depression features (Morton & Miller, 2006; Schmidt et al., 2011).

The San Gabriel Mountains host the most landslide deposits and the most large-landslide deposits relative to the other major ranges in southern California (Morton & Miller, 2006). Morton and Miller (2006) interpret that most of the large landslide deposits in the San Gabriel Mountains are rock avalanche deposits. The largest of these deposits, Crystal Lake Landslide, occurs in the North Fork San Gabriel Canyon and has a length of about 5 km and slightly less than 1 km in width. This deposit, along with other similar style landslide deposits such as the Alpine Canyon Landslide, also in that canyon, were interpreted to be earliest Pleistocene (2.5 Ma) (Morton & Miller, 2006).

A recent study performed in the North Fork San Gabriel Canyon used surface exposure dating to yield absolute dates for the rock avalanche deposits in that canyon. Scherler et al. (2016) were interested in the large terraces formed in the canyons previously interpreted to be caused by climatic events. They were able to link the terraces directly to aggradational sediment pulses from the upstream rock avalanche deposits and

argue that the terraces were a catchment specific feature and not regional. Cosmogenic nuclide dating revealed that the landslides were Holocene; individual boulder dates on surfaces had good age agreement indicating the method produced reliable deposit ages. The Crystal Lake Landslide was dated to be between 8 and 9 ka while the Alpine Canyon Landslide is between 0.6 and 1 ka (Scherler et al., 2016). These ages are up to three order of magnitude younger than previously interpreted by Morton and Miller (2006) (Fig. 9).

Figure 9: A) Map of the North Fork San Gabriel Canyon landslide deposits as mapped by Morton & Miller (2006). They interpreted the landslides to be Qvols, or very old (middle to early Pleistocene; 0.782—2.6 Ma). B) Scherler et al. (2016) used cosmogenic nuclide dating to give an absolute date to the same rock avalanche deposits. The ages from the analysis came back several magnitudes younger than previously interpreted based on field mapping alone.

San Antonio Canyon Rock Avalanches as a Case Study

Rock avalanches can be triggered by earthquakes in areas that have steep hillslopes and fractured bedrock (Keefer et al., 1984). There are rock avalanches that have been mapped by Morton and others (1989) within the San Antonio Canyon. These have been said to be Quaternary in age and were triggered due to climatic events.

Motivation of Study

The rock avalanche deposits in the San Antonio Canyon are very similar to the deposits in the study by Scherler et al. (2016) in terms of morphology, soil development, and vegetation (the term soil development is used in this study to describe the amount of accumulated fine-grained sediments within the void spaces between boulders that could support vegetation growth). If the San Antonio Canyon rock avalanche deposits have similar Holocene ages to the rock avalanche deposits in North Fork San Gabriel Canyon, then hazard assessments should be reconsidered for this area. This case study compliments the Scherler et al. (2016) study by having additional support for Holocene aged rock avalanche deposits in a spatially separate area of the San Gabriel Mountains.

The probability that similar rock avalanches can occur in San Antonio Canyon could be indicated by from the high estimates of expected strong ground shaking and high susceptibility to deep-seated landslides, (Branum et al., 2008; Wills et al., 2011) but would be much better constrained by knowing the ages and recurrence intervals for these large mass wasting events. In addition to the immediate hazard of hillslope failure, it is also important to assess their extent and persistence of hazards arising from the ways that the avalanche deposits modify the fluvial system after coming to rest.

The rock avalanche deposits in the San Antonio Canyon will be dated using cosmogenic nuclide methods. Associated lacustrine and fluvial deposits will be dated using radiocarbon and infrared stimulated luminescence dating. Lidar imagery will be used to map the landslide deposits. This case study compliments the Scherler et al. (2016) study by having additional support for Holocene aged rock avalanche deposits in a spatially separate area of the San Gabriel Mountains.

Methods

Age Determination

Radiocarbon Dating

Radiocarbon dating is a widely used technique to give absolute dates to deposits ranging in age from approximately 50 to 50,000 years before present (e.g., Brock et al., 2010). Sediment packages related to rock avalanche activity were targeted to locate large pieces of charcoal. Rock avalanches have dammed the canyon in the past, creating lacustrine deposits upstream and new fluvial deposits once the rock avalanche was breached. Due to the large amount of fire-prone vegetation, such as the chaparral, in this area, it is likely charcoal is preserved in these sediments and would be ideal for radiocarbon dating. Deltaic lacustrine deposits, post-breach fluvial channels, and terrace deposits were manually searched for single, large pieces of charcoal. To search for smaller pieces of charcoal, sediment from targeted areas were sampled into gallon bags to be processed in the lab.

The lab process involved a float method. Large beakers were filled with deionized water and sediment from the bag was placed into the beaker. Sediment sank while

vegetation and charcoal pieces floated. The float material was collected and allowed to dry in petri dishes. The sediment left over was disposed of. This process was repeated until the entire sample had been treated. Once the float material was dried, the petri dishes were placed under microscopes to then manually search for and collect any charcoal pieces. Non-charcoal organics were not used for radiocarbon dating due to the high errors associated with possible contamination from modern vegetation and roots. Separated charcoal was then shipped to the University of California, Irvine's W.M. Keck Carbon Cycle Accelerator Mass Spectrometry Laboratory for further chemical preparation and analysis. Calibrated ages and uncertainties were determined using OxCal (Ramsey, 2013).

Infrared Stimulated Luminescence Dating

Infrared stimulated luminescence (IRSL) dating estimates the time of sediment burial; i.e. isolation from sunlight (e.g. Wallinga, 2002). The history of the dated feldspar grains is assumed to have been simple. That is, they were exposed to the Sun's ultraviolet radiation for a sufficient time during transport to bleach the grains. Also, after final deposition, the grains were buried quickly and shielded from the Sun's UV radiation. Feldspars are the targeted mineral for IRSL dating. Feldspars accumulate electrons when not exposed to the Sun, but all electrons are freed once the grain is exposed to UV radiation. The rate of electron accumulation is known, allowing burial ages of last exposure to UV radiation to be determined.

Caution is needed to make sure the feldspar grains are not exposed to light at any time during field sampling. A spade or trowel is used to first scrape the outermost surface

of the sediment to remove any bleached grains that can contaminate the sample. A brass sleeve was used to extract and house the sample as follows. A slide hammer was used to pound the brass sleeve into the sediment. Making sure the sample is completely compact and immobile within the sleeve is important. The middle of the sleeve is protected from the sunlight, while the ends are inevitably exposed to the sunlight before being capped with either plastic or rubber and then heavy duty black duct tape. If the sample is not completely compact and immobile, the exposed ends may mix with the unexposed middle, contaminating the sample. If the sample is not compact, one end may be filled with more sediment to make it compact, and a note indicating which end was filled. Essential information compiled for the sites of collection is latitude, longitude, elevation, (which can all be determined by GPS), and notes about the site stratigraphy. Field photographs showing the sleeve in place in context with the sediment and stratigraphy could be useful as well.

There are several steps in preparing the samples for analysis. A dark room, the kind used in photography, is needed to protect the samples from UV exposure. Dimly lit, orange bulbs are sufficient for light and do not expose the samples. The brass sleeves are opened and the outer two centimeters on both sides are scraped off. This eliminates parts of the sample exposed to sunlight during collection. If a sample was filled to make it more compact, the fill material must be removed along with the two centimeters as well. The scraped material is placed into a container labeled "Ends" and weighed. Once weighed, the "Ends" are placed into an oven to dry overnight. The "Ends" are weighed again after being dried to calculate water content. The middle of the sleeves is extracted,

weighed, and placed into a bag labeled "Bulk." The "Bulk" is then sieved to collect the correct size fraction of feldspars for analysis.

A sieve tower is constructed using sieving fabric mesh and plastic funnel-like beakers. Using disposable fabric mesh eliminates sample cross contamination and the time and the risk of mesh distortion involved in cleaning metal sieves. Four to six different fabric mesh opening sizes are used, however the target grain size fraction is between 175 and 200 μm. A handful of the "Bulk" sample is placed into the top sieve of the tower and deionized water under high-pressure is applied while manually shaking the tower. Water is shut off once the top sieve is filled and the tower is manually shaken until the water is evacuated into a plastic collecting container for silt and clay sized material. Another handful of "Bulk" is placed into the tower and the process is repeated until the entire sample is completed. The sediment size fractions are collected into separate bags and dried. All the procedures up to this point were carried out by myself at the University of California, Los Angeles IRSL Laboratory under supervision by Dr. Nathan Brown. The feldspars were then separated by visual inspection from the 175-200 μm fraction and analyzed at UCLA by Dr. Brown.

Cosmogenic Nuclide Dating

Cosmogenic nuclide dating is a surface exposure dating method that gives absolute ages to boulder surfaces ranging in ages from approximately 1,000 to 500,000 years before present (e.g. Ivy-Ochs et al., 2008). Typically used by glacial geomorphologists, this technique has been recently gaining traction for dating terraces and landslide deposits (e.g. Scherler et al. 2016). Rather than dating how long a material

has been blocked from sunlight like IRSL, this method dates how long a surface of a boulder has been exposed. Quartz is the targeted material for this method. Quartz does not naturally have Beryllium-10 (^{10}Be) within its crystal structure, but when exposed to cosmic rays, ^{10}Be starts to accumulate within quartz. The rate of ^{10}Be accumulation in quartz is known, and given the concentration of ^{10}Be in the quartz, it is possible to calculate how long the surface has been exposed to cosmic radiation. The history of the boulder deposited on a landslide surface is assumed to be simple whenever cosmogenic nuclide dating is used. Specific to rock avalanches, the boulder is assumed to have been bulk material within the mass of the mountain side, shielded from radiation before the mass wasting event. After the rock avalanche occurs, the boulder is exposed to cosmic radiation and starts to accumulate ^{10}Be. The boulder is assumed to be on a stable, level original surface of the rock avalanche and does not roll over or move once the rock avalanche is complete. Any weathering of the boulder from wind, rain, ice, plant growth, and spalling from fires is assumed to be minimal, unless observations suggest otherwise, since that would cause the age to be younger than the deposit.

With these assumptions in mind, boulders to be sampled need to be chosen with caution. Targeted boulders need to be stable and on level, original surfaces away from any trails, roads, and slopes. The distal, intact rock avalanche surfaces were targeted since more recent rock falls can occur closer to the source area. It is likely that large boulders that would obstruct roads and trails were moved and rolled by human activity. If a boulder is rolled over or moved, a different surface of the boulder will begin ^{10}Be accumulation, giving a date that is younger than the actual rock avalanche. Once a

surface has been chosen, the next step is to find boulders that are prominent, have a full view of the sky, and are quartz-rich. Having a high concentration of quartz and a more complete view of the sky will result in more accurate absolute ages of the rock avalanche deposit compared to more mafic or shielded boulders. At least two samples were collected from each rock avalanche surface, but ideally three or four samples would be collected.

Before collecting the sample from the targeted boulder, there are other necessary steps. A viewshed measurement must be completed. A viewshed is the actual view of the sky the boulder would have. A digital theodolite was used to obtain the viewshed for each sample. This is done by taking down the change in degrees from horizontal of the skyline from the boulder along with the accompanying azimuth bearing for every 15 azimuth degrees until a full 360-degree coverage is completed. The online CRONUS calculator is used to calculate the topographic shielding (Balco, 2006; Balco et al., 2008). Important information needed to collect is longitude, latitude, elevation and thickness of the sample. The thickness here refers to thickness of the sample being collected. The final thickness for the sample being used for the dating is what is used during the calculations. The rate of ^{10}Be accumulation increases as latitude and elevation increase. The ^{10}Be does not accumulate deep in the rock due to the weak penetration power of cosmic radiation. Due to this, no more than ten-centimeter thick samples of the boulder are needed. It is advisable to collect several kilograms of material and to make sure each boulder is clearly marked in case resampling is needed.

Preparing the samples for CGN dating involves crushing the bulk rock, separating the minerals, and chemical digestion. Chemical digestion is needed to clean, etch, and dissolve the quartz for the ^{10}Be analyses. Due to time constraints and UCR laboratory limitations the chemical digestion steps were completed by the outside lab that analyzed the sample. Dry preparation of the samples is straightforward. Using a rock saw, large samples are cut into chunks that can be crushed in a jaw crusher into small flakes. The flakes are further crushed in an inefficient ring and puck mill pulverizer into the correct size fraction. These steps were completed at UCR. California State University, Northridge allowed use of the lab where a Bico disc mill pulverizer was used to more efficiently crush rock flakes into the correct size fraction between 250 and 500 μm. The next step is to separate the quartz from the rest of the minerals. This was done using a Franz Isodynamic Magnetic Separator. This machine separates minerals based on their magnetic properties. It separates out the quartz from the rest of the minerals with a minor trace amount of feldspars still present. The set-up used for the Franz was a forward tilt toward the user of 12° and a down slope tilt toward the collection cups of 19°. The material was sorted at 1 ampere to begin with and a second run of the sorted material at 1.5 amperes. A 200 g target quartz separate of each sample was sent to the Indiana University Purdue PRIME AMS Laboratory. There, the samples underwent several hydrochloric and hydrofluoric acid baths to clean the quartz and dissolve the remaining feldspars. The samples were then analyzed by AMS. The data that is sent back is entered the CRONUS online calculator to calculate the final absolute age of the samples (Balco, 2006; Balco et al., 2008).

Mapping Methods

Lidar

Lidar is the acronym for light detection and ranging. This technique is useful for creating imagery that has a higher resolution for topographic details than standard aerial imagery does. However, it is not meant for any type of colored, photographic imagery. A lidar unit (laser scanner) is attached to a tripod for terrestrial applications, or in the case of this study, to the underside of an airplane. The laser scanner emits thousands of laser pulses per second. As a laser pulse hits an object it scatters and some of the scatter is sent back to the scanner, which receives the scatter, known as a return. As the laser scanner scans an area laser pulses hit trees, leaves, bushes, rocks, and the ground. After the entire area has been scanned, the raw data is processed into a point cloud of every return. A point cloud is a data set that is compiled of thousands of points generated by the returns. Several useful types of imagery can be created using the point cloud such as digital elevation models and hillshades. Perhaps the most useful aspect of obtaining lidar data is the ability to isolate returns from the point cloud. The point cloud can be processed in such a way that only the last returns, which are ideally the returns of bare ground, are utilized and all other returns from trees, bushes, and other undesirable points are removed. This reveals subtle surface relief that would be obscured by vegetation to become apparent (e.g. Jaboyedoff et al., 2012).

Lidar Datasets

LARIAC

The LARIAC4 lidar data are provided by Los Angeles County and the USGS. Drew Decker (USGS) was able to get us the data needed for this study from the LARIAC4 dataset. Airborne lidar was flown over the entire LA County in 2015 for an approximate area total of 150 km^2. The point density was about 2-3 points per square-meter creating a quality level 2 (QL2) product, a DEM with 1-meter resolution (Graham, 2015). This dataset defaults to the Imperial measurement system where the elevation was measured in feet.

NCALM

The NCALM data was acquired by a grant given to Christopher Gentile directly from NCALM through their seed proposal program. They flew airborne lidar in October of 2017 over ~70 km^2 of the eastern portion of the canyon. The area chosen for this grant was deliberately chosen to adjoin the LARIAC lidar dataset. The point density is about 3-4 points per square-meter creating a QL2 quality DEM with 1-meter resolution. The dataset defaults to the Metric measurement system where elevation was measured in meters.

Geographic Information Systems

FieldMove

FieldMove is a commercial digital geologic mapping application that allows the user to create lines, paths, polygons, and localities while in the field. Pictures, notes and measurements can be attached to specific localities. All field work was done using this

application to record information and placemark localities of samples. Basemaps were created from caltopo.com and imported into the FieldMove application. Google Earth .kmz files were exported from the maps created using this software.

Google Earth Pro

Google Earth Pro is a free geographic information system (GIS) software. Paths, lines, polygons and placemarks can be created and saved. Simple spatial analysis tools are available as well. Detailed aerial imagery is available as a basemap. Rotating the view with respect to topography and adding vertical exaggeration are very useful for identifying and mapping landslide deposits.

ArcMap

ArcMap is a commonly used geographic information system software. The user has the capabilities to create features in raster or vector shapefile formats. Examples of raster data would be digital elevation models (DEM), GeoTIFF files, hillshade maps, and lidar imagery. Vector shapefiles are features such as polygons and lines. Many tools are available for creating derivative products or analyzing data.

NCALM delivered the lidar data as a single DEM. LARIAC, however, delivered their lidar DEM in tiled files. The tiles had to be mosaicked together in ArcMap before creating a DEM. The ArcMap tool "Mosaic to New Raster" under the "Raster Dataset" tab within the "Data Management Tools" toolbox performs this function. In the "Mosaic to New Raster" window, the LARIAC .img files were input into the tool. Next the output folder was selected, and an appropriate name created. Under the "Pixel Type" drop-down menu, "32_BIT_FLOAT" was selected. The "Number of Bands" chosen was "1" and the

tool was run. This created a single DEM file. However, the NCALM DEM and the LARIAC mosaicked DEM could not be mosaicked together in the same operation. All maps created from the DEMs thereafter had to be created twice, once with each dataset, then those were mosaicked together. Slope, aspect, and various hill-shade maps were created.

Deposit Observations

Field observations of the five main rock avalanche deposits in the upper San Antonio Canyon catchment are detailed in the following sections (Fig. 10). The landslides are described from the highest source area in the catchment to the lowest. Table 1 summarizes the rock avalanches' characteristics, inferred relative ages, age classifications, and age constraints.

Three age classifications (young, mature, old) are defined based off of several features of the deposits such as preservation of headscarp and original surfaces, weathering of boulders on original surfaces, accumulation of fine-grained sediment in void spaces, vegetation growth, and amount of incision and erosion of deposit material. This age classification scheme may not apply to deposits in other areas outside of San Antonio Canyon that experience different climates, topography, or vegetation.

(1) Young deposits have defined headscarps, well-preserved original surfaces with angular to sub-angular boulders, and large, deep void spaces between boulders with no to minimal fine-grained sediment accumulation. There is very little vegetation growth made up of mainly large conifers on the distal portion of the deposit and little incision into the deposit with the morphology mostly intact and preserved.
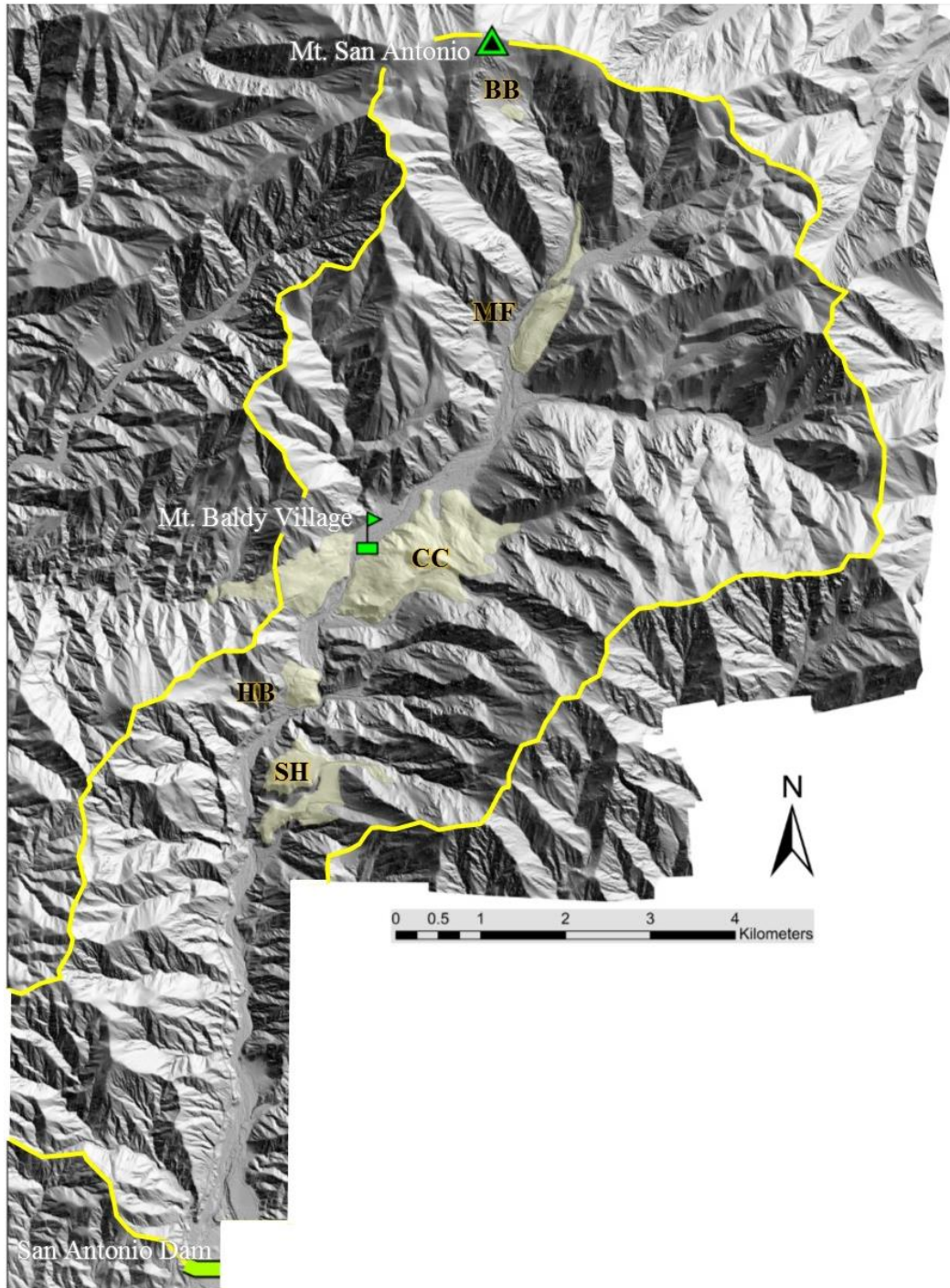
Figure 10: Lidar hillshade overview of the San Antonio Canyon catchment (outlined in yellow). The five major rock avalanche deposits are labeled and mapped in pale yellow. Major landmarks of the canyon are labeled as well. Unfortunately, a couple small sections of the lidar data was corrupted so the San Antonio Dam has been cut in half. Deposit abbreviations are as follows:
BB– Baldy Bowl, CC– Cow Canyon Saddle, - HB– Hog Back, MF– Manker Flats, SH– Spring Hill.

(2) Mature deposits may have headscarps that are difficult to define and some lost original surfaces. The boulders on the original surfaces that are still preserved are angular to sub-angular with some void space between them. The void spaces have some accumulation of fine-grained sediments that allow vegetation, such as small shrubs and chaparral, to grow along with the large conifers. The deposits could be bisected by the main drainage with minimal headward incision, but the majority of the morphology is preserved.

(3) Old deposits have non-existent, or nearly non-existent, headscarps with minimal to no original surfaces preserved. Boulders are sub- to well-rounded with exfoliation and spalling present and could have discoloration and weathering rinds. Boulders are sparse and sit on a thick accumulation of fine-grained sediment that promote dense vegetation growth. The vegetation is similar to the normal vegetation of the canyon in that there is mostly chaparral and shrubs with no large conifers at low latitudes and sparse conifers at higher altitudes. There is a considerable amount of erosion of the deposit and the drainage has completely or mostly returned to equilibrium. There is significant incision headward creating small catchments within the deposit.

Baldy Bowl Avalanche

The Baldy Bowl rock avalanche deposit has the smallest area and volume of the five deposits at about 0.038 km^2 and 6.25x10^6 m^3 respectively. The landslide had a fall height (H) of about 550 m and a runout distance (L) of about 900 m yielding a H:L ratio of 0.6, the highest of the landslides studied. The deposit is well preserved; there are no outcrops below the boulder cap that expose internal textures. The surface boulders are up

Deposit	Deposit Remaining Area (km^2)	Deposit Volume (m^3)	Estimated Volume of Eroded Material (m^3)	Fall Height, H (m)	Runout Distance, L (m)	H:L Ratio
Baldy Bowl	0.038	6.25×10^6	0	550	900	0.60
Manker Flat	0.54	3.24×10^7	1.62×10^7	1400	4000	0.35
Cow Canyon Saddle	2.41	3.6×10^8	1.63×10^8	1400	4900	0.28
Hog Back	0.20	1.4×10^7	4.68×10^6	500	1100	0.45
Spring Hill	0.69	7.14×10^7	1.62×10^9	1100	3300	0.33

	Lake Area (km^2)	Relative Age 1= Oldest 5= Youngest	Age Classification	Deposit Age Constraint
Baldy Bowl	0	5	Young	< 4 ka
Manker Flat	0	3	Mature	500 yr < MF < 4 ka
Cow Canyon Saddle	1.33	2	Mature	4039 ±491 years old
Hog Back	0.154	4	Young	500 yr < HB < 4 ka
Spring Hill	0.373	1	Old	< 45 ka

Table 1: Characteristics of the five rock avalanche deposits studied in San Antonio Canyon.

to 5 m on a side and angular with sharp edges that show no significant signs of weathering or spalling. The boulders are loosely packed with significant pore space between the boulders (voids that extend several meters below the surface). There is very little accumulation of fine material following deposition of the deposit, suggesting a youthful age. The deposit is void of vegetation apart from a few sparse large, conifers. This deposit is located 920 m southeast from Mt. San Antonio Peak, (the highest point in the San Gabriel Mountains) and has a clear source area from the broad amphitheater-shaped headscarp 600 m south of the Mt. San Antonio Peak. This headscarp region is largely void of vegetation and is actively shedding scree. Several debris flow chutes with levees traverse the source area and are deflected around the Baldy Bowl deposit. This deposit can be covered with snow from December or January until June or July. The south side of the Mt. San Antonio Peak may block some of the direct sunlight to the deposit.

Manker Flat Avalanche

The Manker Flat deposit has an area of 0.54 km^2 and a volume of 3.24x10^7 m^3. The source area for this rock avalanche was the southeast flank of Mt. San Antonio Peak at about 3,000 m elevation. The landslide traveled down San Antonio Canyon (over the region that is now San Antonio Falls) and past Manker Canyon. The area named Manker Flat on topographic maps is actually the region of alluvium in Manker Canyon impounded behind the Manker Flat rock avalanche deposit. Manker Creek incises steeply through the deposit to rejoin San Antonio Creek, dividing the deposit into two main extents. As noted by Morton et al. (1989) there appear to be eroded remnants of this landslide deposit above San Antonio Falls, such as where the Mt Baldy Trail crosses at about 2,300 m elevation. The blunt toe of the Manker Flat rock avalanche deposit is well preserved; it is a lateral distance of 4,000 m away from its source area and 1,400 m lower in elevation indicating an H:L ratio of 0.35. There has been considerable human development built on this deposit including a major switchbacking road and over a hundred private cabins. Where the original landslide surface is preserved the boulders are angular and show little signs of any significant weathering or spalling. Interstitial space between the boulders is rare and there is enough accumulation of fine material to promote a combination of chaparral, shrubs, and the typical large conifers seen on rock avalanche deposits. There appears to be outcrop of internal rock avalanche shearing and jigsaw textures at the river channel level that were seen at a distance but not accessed. Several of the roadcuts at the switchback corners expose internal rock avalanche textures, especially the roadcut just east of the Iron Gate Road junction.

Cow Canyon Saddle Avalanche

This is the largest rock avalanche deposit recognized in San Antonio Canyon, at about 2.41 km^2 for area and 3.6x10^8 m^3 for volume, and one of the largest known in the San Gabriel Mountains. This rock avalanche came from two source areas on the east side of the drainage (southwest of Ontario Peak at 2,650 m elevation), traveled laterally across San Antonio and dammed the valley to a height of at least 100 m. The landslide deposit comprises the saddle between San Antonio Canyon and Cow Canyon to the west (Cow Canyon Saddle). The toe of the landslide is well preserved in the head of the Cow Canyon which allow accurate fall height and runout distances to be determined. The landslide had a fall height (H) of about 1,400 m and a runout distance (L) of about 4,900 m, yielding a H:L ratio of 0.28, the lowest of the landslides studied.

The Cow Canyon Saddle avalanche deposit itself has been subsequently bisected by erosion. The portion of the deposit east of the drainage has been incised headward. There is some evidence of original boulder cap surface on the east side, but the most intact boulder cap surfaces are on the west deposit near Cow Canyon Saddle, which is where cosmogenic sampling was targeted. The surface on the west deposit is flat with angular boulders that are predominantly quartzites. There are patches of original surface without vegetation that have little accumulation of fine material and gaps between boulders up to one meter deep. Between these surfaces there is chaparral, shrubs, and conifers. There is considerable accumulation of fine material such that grasses grow on both deposits.

The east deposit does not show signs of well-preserved original boulder cap surface and may have been more prone to wildfires in the past. While the eastern deposit may not have the desirable original surfaces, there are excellent outcrops of internal rock avalanche textures, especially in the tall road cut north of the Mt. Baldy Fish Ponds. The mixed zone exhibits shearing and jigsaw puzzle textures.

Hog Back Avalanche

The Hog Back rock avalanche deposit is relatively small at about 0.20 km^2 for area and 1.4×10^7 m^3 for volume. The landslide has a clear source area on the west side of the canyon and traveled in a southeast direction to cross San Antonio Canyon and create a topographic barrier at least 50 m in height. The landslide had a fall height (H) of about 500 m and a runout distance (L) of about 1,100 m, yielding a H:L ratio of 0.45. In contrast to the Baldy Bowl, Manker Flat, and Cow Canyon Saddle landslides, the Hog Back rock avalanche was stopped by the opposing canyon wall but potentially had the capability of traveling further. The deposit has well-preserved topographic form with a well preserved original boulder cap surface. The boulders are large, angular and show no signs of significant weathering or spalling, even though some of the tree trunks have burn marks on the bark. There is little to no accumulation of fine material between the boulders and in many cases void spaces extend at least two meters beneath the surface. The vegetation is mostly tall conifers with some shrubs more proximal to the source area. There are some outcrop showing internal textures along the main road and the old abandoned road.

The Hog Back rock avalanche buried the former channel of San Antonio Creek. The creek is currently cutting a new gorge (epigenetic gorge) into bedrock at the eastern margin of the deposit. This knickzone contains a 10 m high waterfall and drops over 25 m in a distance of 200 m.

Spring Hill Avalanche

The Spring Hill rock avalanche deposit is relatively large, 0.69 km^2 for area and 7.14x10^7 m^3 for volume. It has a source area at the head of Cascade Canyon at about 2,000 m and traveled northwest out of the canyon and across San Antonio Canyon. Although the deposit appears to only be preserved on the eastern side of the canyon, extrapolation of the slope of the deposit indicates the landslide very likely spanned the canyon and ran into the western wall of the canyon. Its toe is not preserved but if the landslide is assumed to have reached the west side of the canyon then the best estimates are that it had a fall height (H) of about 1,100 m and a runout distance (L) of about 3,300 m, yielding a H:L ratio of 0.33.

Several lines of evidence suggest this is the oldest of the five deposits examined. Boulders are rare on the low gradient surface of the deposit, indicating poor preservation of the landslide's boulder cap. The boulders are sub- to well-rounded and have a significant weathering rind. The boulders have experienced significant spalling from past wildfires. The vegetation is mostly grasses with sparse shrubs in the proximal part of the deposit. The distal area, where the boulders are located, is mostly chaparral with considerable poison oak. A large dry drainage is incised into the deposit south of the 4,056' Spring Hill spot height; Cascade Creek also incises through the deposit. Looking

with binoculars across from the Mt Baldy Road reveals that the deposit is consolidated enough that it forms vertical cliffs with red weathering that is not present in any of the other landslide deposits observed. These outcrops were not visited due to the difficult access. Bedrock is exposed beneath the Spring Hill deposit, suggesting considerable downcutting of San Antonio Canyon since the time the landslide occurred. Other than at the Hog Back, the narrowest and most sinuous part of the main San Antonio Canyon is near the southern margin of the Spring Hill deposit; two tunnels were even needed to be built to put the Mt Baldy Road through this area. A possible interpretation is that the active San Antonio Creek channel was an epigenetic gorge that bypassed the landslide deposit and that the former valley bottom is buried beneath the main Spring Hill deposit but more detailed mapping would need to be done to confirm this.

Geochronology

Geochronology samples are summarized in Table 2.

AMS Radiocarbon

One piece of charcoal from post-Hog Back rock avalanche lacustrine sediments was selected. The sample age is 2225 ±15 years BP.

Infrared Stimulated Luminescence

Three samples from post-Hog Back rock avalanche sediments were analyzed. Preliminary results from the samples suggest ages between 4 and 5 ka. Further analysis is currently being performed at UCLA.

Sample	Deposit	Sampling Type	Elevation (m)	Latitude	Longitude	Age
C171210B1	Baldy Bowl	10Be/Cosmo	2495.3	34.27975	-117.64092	In Progress
C171210B2	Baldy Bowl	10Be/Cosmo	2532.3	34.28047	-117.64189	In Progress
C171015B4	Manker Flat	10Be/Cosmo	1812.0	34.26075	-117.63453	In Progress
C171022B1	Manker Flat	10Be/Cosmo	1637.1	34.25452	-117.63919	In Progress
C171022B3	Manker Flat	10Be/Cosmo	1674.3	34.25586	-117.63849	In Progress
C171022B4	Manker Flat	10Be/Cosmo	1724.6	34.25794	-117.63756	In Progress
N160802A	Cow Canyon	10Be/Cosmo	1413.7	34.22903	-117.66977	**4097 ±478***
N160802B	Cow Canyon	10Be/Cosmo	1403.0	34.22957	-117.67006	**3981 ±503***
N171212A	Cow Canyon	10Be/Cosmo	1376.2	34.23000	-117.66990	In Progress
N171212B	Cow Canyon	10Be/Cosmo	1374.0	34.23023	-117.66986	In Progress
C161022B2	Hog Back	10Be/Cosmo	1171.7	34.22010	-117.66667	In Progress
C170204B1	Hog Back	10Be/Cosmo	1164.3	34.21881	-117.66734	In Progress
C171015B1	Hog Back	10Be/Cosmo	1167.4	34.22054	-117.66760	In Progress
C17024L1	Hog Back	IRSL	1137.0	34.22063	-117.66486	In Progress
N171221A	Hog Back	IRSL	1142.0	34.22180	-117.66550	In Progress
N171221B	Hog Back	IRSL	1130.0	34.21976	-117.66579	In Progress
N160729D	Hog Back	Radiocarbon	1141.0	34.22235	-117.66496	**2225 ±15+**
C170305B1	Spring Hill	10Be/Cosmo	1221.3	34.20966	-117.66764	In Progress
C170305B2	Spring Hill	10Be/Cosmo	1218.6	34.20953	-117.66794	In Progress

Table 2: Samples for dating. This table shows the samples collected, their related deposit, associated method, elevation, latitude, longitude, and their ages. Ages have been bolded while those still awaiting processing and analysis are labeled as "In Progress."
* 10Be/Cosmogenic Nuclide ages are surface exposure ages since present.
+ Radiocarbon dates are calibrated years BP (Before Present, which is 1950).

Cosmogenic Nuclide Dating

Two samples were collected from the Baldy Bowl rock avalanche deposit and are currently being analyzed. Four samples were collected from the Manker Flat rock avalanche deposit and are currently being analyzed. Four samples were collected from the Cow Canyon Saddle rock avalanche deposit; two are currently being analyzed. Two

of the samples yielded dates of 4097 ±478 and 3981 ±503 years. These are being used to give a preliminary date of 4039 ±491 years for the Cow Canyon Saddle deposit until the other ages are available. Three samples were collected from the Hog Back rock avalanche deposit and are currently being analyzed. Two samples were collected from the Spring Hill rock avalanche deposit and are currently being analyzed. These two boulders have considerable spalling from multiple fires throughout their history so the resulting exposure ages will be considered minimum ages for the Spring Hill deposit.

Discussion

Age of Rock Avalanches in San Antonio Canyon

Understanding the timing of rock avalanche events in San Antonio Canyon is still in progress as dates from this study are still being acquired and finalized. The preliminary data is able to confirm that these deposits are much younger than previously thought (e.g. late Holocene rather than early Pleistocene).

Early geochronological results suggest the deposits are several orders of magnitudes younger than the original estimate of early Pleistocene. Even though these deposits are Holocene, there is a considerable amount of incision and erosion, such as the fluvial cutting of Manker Flat and Cow Canyon Saddle deposits. This would suggest that San Antonio Canyon is a more dynamic and active area than previously thought. If the finalized dates for the Cow Canyon Saddle deposit are approximately 4 ka, similar to those obtained for the Crystal Lake Landslide, this could suggest a common triggering event. The Cow Canyon Saddle deposit has two source areas with no evidence of two separate failure events combining to form the total deposit. This supports the possibility

that the triggering event may be an earthquake rather than an extreme weather event. This is speculative until further dates can be analyzed from around the San Gabriel Mountains; the timing does not correlate to any known climatic events (Scherler et al., 2016).

Having a range of deposit ages (see young, mature, old classifications) within the same canyon allows us to understand the evolution of rock avalanche deposits in terms of their morphology and sediment contribution. As the deposits age, they tend to lose their headscarp, morphology, and original surfaces while there is an increase in accumulation of fine-grained sediments, vegetation, and incision and erosion. The young deposits, Baldy Bowl and Hog Back, have 0% and 25%, respectively, of their original material eroded. The mature deposits, Manker Flat and Cow Canyon Saddle, have 33% and 31%, respectively, of their material eroded. The old Spring Hill deposit has lost about 95% of its original material to erosion. Combining this information with absolute ages will give a rate of erosion for the unconsolidated deposits within San Antonio Canyon.

The rock avalanche deposits have lasting effects on the San Antonio Creek channel. The channel becomes more narrow and steeper through the deposits than it normally is. The Hog Back deposit is young and the channel is currently the steepest and most narrow through this area. The oldest deposit, Spring Hill, appears to not affect the channel any longer. The creek through the Spring Hill area is at equilibrium and is relatively wide. This gives us constraints on how long lasting the rock avalanche deposits effect the drainage.

The recurrence interval appears to be on the order of one large rock avalanche every 1000 years potentially. The Hog Back deposit is young, possibly the same age as the Alpine Landslide deposit (0.6-1 ka) (Scherler et al., 2016). This suggests that the area may experience another rock avalanche soon.

Hazard Assessment of Rock Avalanches in San Antonio Canyon

Rock avalanches, on their own, represent a catastrophic hazard that is very damaging and deadly (Keefer et al., 1984). However, there are other hazards associated with the rock avalanche deposits. The deposits dam drainages, which flood valleys upstream to cause lakes. If the lake breaches the deposit it can cause flooding and sediment pulses downstream. The deposit, also, creates a large supply of unconsolidated material that is easily eroded and can be a source for debris flows to occur (Scherler et al., 2016).

Potential extent of lakes impounded behind the rock avalanche deposits were mapped in ArcMap by using the deposits' modern elevation of remnant original boulder cap surfaces that help define the original shape of the deposit (Fig. 11). The Baldy Bowl and Manker Flat deposits had no impounded lake upstream. The Cow Canyon Saddle impounded lake flooded about 2 km upstream for a total area of about 1.33 km^2. The Hog Back rock avalanche deposit created a lake with an area about 0.154 km^2 and flooded 0.75 km of the valley length upstream. The Spring Hill deposit's dammed lake had an area about 0.373 km^2 and flooded the area up about 1 km upstream from the deposit.
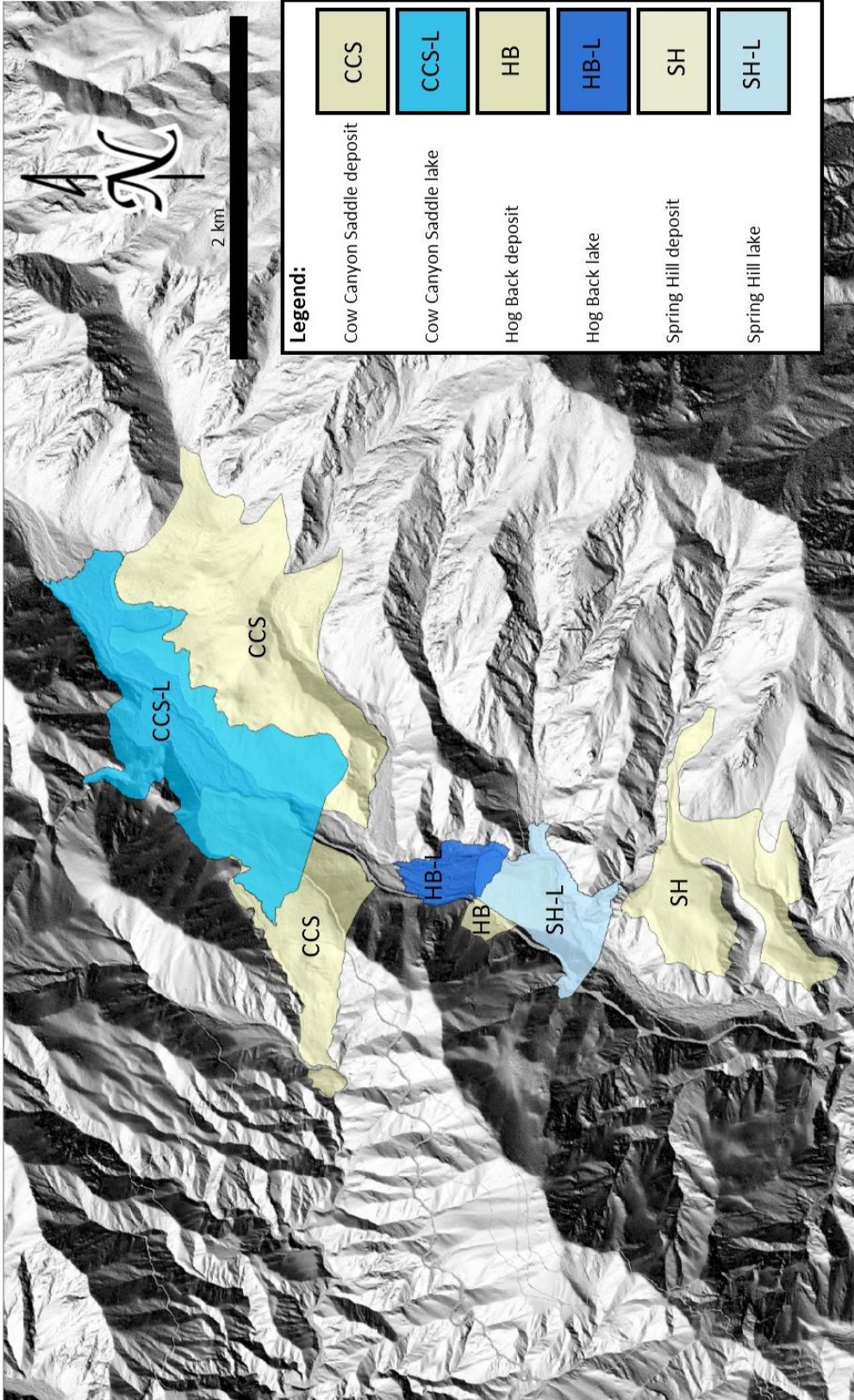
Figure 11: The three rock avalanche deposits (in pale yellow) along with their associated impounded lake (shades of pale blue). The Spring Hill lake covers the area that the Hog Back deposit now occupies, but it would have existed before the Hog Back rock avalanche.

Conclusion

Five landslide deposits were examined in San Antonio Canyon and found to be considerably younger than previously estimated - Late Holocene to Late Pleistocene (0.5 ka to <45 ka) instead of Early Quaternary (100 ka to 2.6 Ma). Fall height to runout length ratios (H:L) for the landslides range from 0.28 for Cow Canyon Saddle to 0.61 for Baldy Bowl, consistent with these landslides being classified as rock avalanches. The largest rock avalanche deposit, Cow Canyon Saddle, has a ^{10}Be exposure age of 4039 ± 491 yrs. Using available absolute age constraints and a preservation classification scheme considering geomorphology, accumulation of fine material and vegetation, the relative ages of the landslides were interpreted to be (from oldest to youngest) Spring Hill, Cow Canyon Saddle, Manker Flat, Hog Back, Baldy Bowl.

Together the five deposits represent about 0.5 km^3 of material being stored; there is a strong correlation between the age of the deposit and the volume of the deposit that has been subsequently removed by erosion. Aggradational terraces downstream of these landslide deposits may be linked to these landslide deposits and thus also be younger than assumed. Three of the rock avalanche deposits have morphologies that indicate that extensive lakes to 1.3 km^2 may have formed upstream of the deposits; there are sedimentary deposits that indicate a lake formed behind the Hog Back rock avalanche to its spillover elevation. Though the recurrence of rock avalanches in San Antonio Canyon is relatively low (four in the last four thousand years) compared to debris flows (annual to decadal), their affects are large by comparison. The record (and erosion) of large rock avalanches in San Antonio Canyon indicate that the landscape overall is more active and

dynamic than previously assumed. The recency of the deposits indicate that earthquake-triggered landslides may be an important landscape driver over a millennial time period.

References

Balco, G. (2006). CRONUS Calculators. Retrieved June 12, 2018, from
      https:hess.ess.washington.edu/

Balco, G., Stone, J.O., Lifton, N.A., & Dunai, T.J. (2008). A complete and easily
      accessible means of calculating surface exposure ages or erosion rates from [10]Be
      and [26]Al measurements. *Quaternary Geochronology, 3*, 174-195.

Barth, N.C. (2013). The Cascade rock avalanche: Implications of a very large Alpine
      Fault-triggered failure, New Zealand. *Landslides, 11*, 327-341.

Beck, A.C. (1968). Gravity faulting as a mechanism of topographic adjustment. *New
      Zealand Journal of Geology and Geophysics, 11*(1), 191-199.

Blythe, A.E., Burbank, D.W., Farley, K.A., & Fielding, E.J. (2000). Structural and
      topographic evolution of the central Transverse Ranges, California, from apatite
      fission-track, (U-Th)/He and digital elevation model analyses. *Basin Research,
      12*, 97-114.

Blythe, A.E., House, M.A., & Spotila, J.A. (2002). Low-temperature thermochronology
      of the San Gabriel and San Bernardino Mountains, Southern California:
      Constraining structural evolution, *in* Barth, A. (ed), *Contributions to Crustal
      Evolution of the Southwestern United States:* Boulder, Colorado, Geological
      Society of America Special Paper 365, 231-250.

Branum, D., Harmsen, S., Kalkan, E., Petersen, M., & Wills, C. (2008). Earthquake
      shaking potential for California. *California Geological Survey, Map Sheet 48
      (Revised 2008).*

Brock, F., Higham, T., Ditchfield, P., & Ramsey, C.B. (2010). Current pretreatment
      methods for AMS radiocarbon dating at the Oxford Radiocarbon Accelerator Unit
      (ORAU). *Radiocarbon, 52*(1), 103-112.

Burns, C., & Sauer, J. (1992). Resistance by natural vegetation in the San Gabriel
      Mountains of California to invasion by introduced conifers. *Global Ecology and
      Biogeography Letters, 2*(2), 46-51.

Cannon, S.H., & DeGraff, J. (2009). Chapter 9: The increasing wildfire and post-fire
      debris-flow threat in western USA, and implications for consequences of climate
      change *in* Sassa, K. & Canuti, P. (eds), *Landslide-Disaster Risk Reduction*, 177-
      190.

Chigira, M., & Kiho, K. (1994). Deep-seated rockslide avalanches preceded by mass rock creep of sedimentary rocks in the Akaishi Mountains, central Japan. *Engineering Geology, 38*, 221-230.

Graham, L. (2015). LIDAR quality level-Part 1 [PDF file]. *The Reference Library*, 1-5. Retrieved from support.geocue.com/wp-content/uploads/2015/07/LIDAR-Quality-Levels.pdf

Hungr, O., Evans, S.G., Bovis, M., & Hutchinson, J.N. (2001). A review of the classification of landslides of the flow type. *Environmental and Engineering Geoscience, 7*(3), 221-238.

Hungr, O., Leroueil, S., & Picarelli, L. (2014). The Varnes classification of landslide types, an update. *Landslides, 11*, 167-194.

Ivy-Ochs, S., & Kober, F. (2008). Surface exposure dating with cosmogenic nuclides. *Quaternary Science Journal, 57/1-2*, 179-209.

Jaboyedoff, M., Oppikofer, T., Abellán, A., Derron, M.H., Loye, A., Metzger, R., & Pedrazzini, A. (2012). Use of LIDAR in landslide investigations: a review. *Natural Hazards, 61*, 5-28.

Keefer, D.K. (1984). Landslides caused by earthquakes. *Geological Society of America Bulletin, 95*, 406-421.

Kirby, M.E., Lund, S.P., Anderson, M.A., & Bird, B.W. (2007). Insolation forcing of Holocene climate change in Southern California: A sediment study from Lake Elsinore. *Journal of Paleolimnology, 38*, 395-417.

Landslide Classification Image. (2017) [Chart of material and movement for landslides modified from Varnes, 1978]. *How does BGS classify landslides?* Retrieved from http://www.bgs.ac.uk/landslides/how_does_bgs_classify_landslides.html

Lave, J., & Burbank, D. (2004). Denudation processes and rates in the Transverse Ranges, southern California: Erosional response of a transitional landscape to external and anthropogenic forcing. *Journal of Geophysical Research: Earth Surface, 109*, 1-31.

Lifton, N.A., & Chase, C.G. (1992). Tectonic, climatic and lithologic influences on landscape fractal dimension and hypsometry: Implications for landscape evolution in the San Gabriel Mountains, California. *Geomorphology, 5*(1-2), 77-114.

Luyendyk, B.P. (1991). A model for Neogene crustal rotations, transtension, and transpression in southern California. *Geological Society of America Bulletin, 103*, 1528-1536.

Matti, J.C., & Morton, D.M. (1993). Paleogeographic evolution of the San Andreas fault in Southern California: A reconstruction based on a new cross-fault correlation, *in* Powell, R.E. et al. (eds), *The San Andreas Fault System, Displacement Palinspastic Reconstruction, and Geologic Evolution:* Geological Society of America Memoir 178, 107-159.

McCalpin, J.P. (1999). Criteria for determining the seismic significance of sackungen and other scarp like landforms in mountainous regions. *Techniques for Identifying Faults and Determining their Origins. US Nuclear Regulatory Commission, Washington*, 2-55.

Moore, J.R., Pankow, K.L., Ford, S.R., Koper, K.D., Hale, J.M., Aaron, J., & Larsen, C.F. (2017). Dynamics of the Bingham Canyon rock avalanches (Utah, USA) resolved from topographic, seismic, and infrasound data. *Journal of Geophysical Research: Earth Surface, 122*, 615-640.

Morton, D.M., Sadler, P.M., & Minnich, R.A. (1989). Large rock-avalanche deposits: Examples from the central and eastern San Gabriel Mountains of southern California. *Publications of the Inland Geological Society, 2*, 323-337.

Morton, D.M., & Miller, F.K. Digital Preparation by Cossette, P.M., & Bovard, K.R. (2006) Geologic map of the San Bernardino and the Santa Ana 30' x 60' quadrangles, California. *US Geological Survey, 1217*.

Muir, J. (1918). *Steep trails*. Boston and New York: Houghton Mifflin Company.

Nicholson, C., Sorlien, C.C., Atwater, T., & Luyendyk, B.P. (1994). Microplate capture, rotation of the western Transverse Ranges, and initiation of the San Andreas transform as a low-angle fault system. *Geology, 22*, 491-495.

National Oceanic and Atmospheric Administration (NOAA). (2018). *California Nevada River Forecast Center*. Retrieved from https://www.cnrfc.noaa.gov/ol.php?type=precip.

Nourse, J.A. (2002). Middle Miocene reconstruction of the central and eastern San Gabriel Mountains, southern California, with implications for evolution of the San Gabriel fault and Los Angeles basin, *in* Barth, A. (ed), *Contributions to Crustal Evolution of the Southwestern United States:* Boulder, Colorado, Geological Society of America Special Paper 365, 161-185.

Olsen, K.B., Day, S.M., Minster, J.B., Cui, Y., Chourasia, A., Faerman, M., Moore, R., Maechling, P., & Jordan, T. (2006). Strong shaking in Los Angeles expected from southern San Andreas earthquake. *Geophysical Research Letters, 33*, 1-4.

Owen, L.A., Finkel, R.C., Minnich, R.A., and Perez, A.E. (2003). Extreme southwestern margin of late Quaternary glaciation in North America: Timing and controls. *Geology, 31*(8), 729-732.

Ramsey, C.B., & Lee, S. (2013). Recent and planned developments of the program OxCal. *Radiocarbon, 55*(2-3), 720-730.

Rulli, M.C., & Rosso, R. (2005). Modeling catchment erosion after wildfires in the San Gabriel Mountains of southern California. *Geophysical Research Letters, 32*, 1-4.

Scherler, D., Lamb, M.P., Rhodes, E.J., & Avouac, J.P. (2016). Climate-change versus landslide origin of fill terraces in a rapidly eroding bedrock landscape: San Gabriel River, California. *Geological Society of America Bulletin.*

Schmidt, K.M., Hanshaw, M.N., Howle, J.F., Kean, J.W., Staley, D.M., Stock, J.D., & Bawdeng, W. (2011). Hydrologic conditions and terrestrial laser scanning of post-fire debris flows in the San Gabriel Mountains, CA, U.S.A. *Italian Journal of Engineering Geology and Environment,* 583-593.

Stuart, J. D., & Sawyer, J. O. (2001). *Trees and shrubs of California* (Vol. 62). Univ of California Press.

Sykes, L.R., & Nishenko, S.P. (1984). Probablities of occurrence of large plate rupturing earthquakes for the San Andreas, San Jacinto, and Imperial faults, California, 1983-2003. *Journal of Geophysical Research, 89*(B7), 5905-5927.

Tchakerian, V.P., & Lancaster, N. (2002). Late Quaternary arid/humid cycles in the Mojave Desert and western great Basin of North America. *Quaternary Science Reviews, 21*, 799-810.

Tucker, A.Z., & Dolan, J.F. (2001). Paleoseismologic evidence for a >8 ka age of the most recent surface rupture on the eastern Sierra Madre fault, northern Los Angeles region, California. *Bulletin of the Seismological Society of America, 91*(2), 232-249.

Ulrich, T. (1987). Stability of rock protection on slopes. *Journal of Hydraulic Engineering, 113*(7), 879-891.

United States Geological Survey (USGS). (2018). *USGS Surface-Water Annual Statistics for California.* Retrieved from https://waterdata.usgs.gov/ca/nwis/annual/?referred_module=sw&site_no=1 1073000&por_11073000_8163=2207769,00060,8163,1901,1972&year _type=W&format=html_table&date_format=YYYY-MM-DD&rdb_compression=value&submitted_form=parameter_selection_li st

Varnes, D.J. (1978). Slope Movement Types and Processes. In *Landslides: Analysis and Control* (Special Report 176, pp. 11-33). Transportation Research Board.

Wallinga, J. (2002). Optically stimulated luminescence dating of fluvial deposits: a review. *Boreas, 31*, 303-322.

Weldon, R., & Humphreys, E. (1986). A kinematic model of southern California. *Tectonics, 5*(1), 33-48.

Wills, C.J., Perez, F.G., & Gutierrez, C.I. (2011). Susceptibility to deep-seated landslides in California. *California Geological Survey, Map Sheet 58.*

Yarnold, J.C., & Lombard, J.P. (1989). Facies model for large block avalanche deposits formed in dry climates in Colburn, I.P., Abbott, P.L., & Minch, J. (eds), *Conglomerates in Basin Analysis: SEPM Pacific Section Symposium Book, 62*, 9-32.